

HIGGS SEARCHES IN ATLAS

A. SCHAFFER

On behalf of the ATLAS Collaboration

LAL, Univ Paris-Sud, IN2P3/CNRS

Orsay, France

E-mail: R.D.Schaffer@cern.ch

This talk covers the results of a search for the Standard Model Higgs boson in proton-proton collisions with the ATLAS detector at the LHC. The datasets used correspond to integrated luminosities of approximately 4.8 fb^{-1} collected at $\sqrt{s} = 7 \text{ TeV}$ in 2011 and 5.8 fb^{-1} at $\sqrt{s} = 8 \text{ TeV}$ in 2012. Individual searches in the channels $H \rightarrow ZZ^{(*)} \rightarrow 4\ell$, $H \rightarrow \gamma\gamma$ and $H \rightarrow WW^{(*)} \rightarrow e\nu\mu\nu$ in the 8 TeV data are combined with previously published results of searches for $H \rightarrow ZZ^{(*)}$, $WW^{(*)}$, $b\bar{b}$ and $\tau^+\tau^-$ in the 7 TeV data and results from improved analyses of the $H \rightarrow ZZ^{(*)} \rightarrow 4\ell$ and $H \rightarrow \gamma\gamma$ channels in the 7 TeV data. Clear evidence for the production of a neutral boson with a measured mass of $126.0 \pm 0.4 \text{ (stat)} \pm 0.4 \text{ (sys)} \text{ GeV}$ is presented. This observation, which has a significance of 5.9 standard deviations, corresponding to a background fluctuation probability of 1.7×10^{-9} , is compatible with the production and decay of the Standard Model Higgs boson. First measurements of the couplings of this particle are presented and are compatible with a SM Higgs boson hypothesis.

1 Introduction

The Standard Model (SM) of particle physics [1–4] has been tested by many experiments over the last four decades and has been shown to successfully describe high energy particle interactions. However, the mechanism that breaks electroweak symmetry in the SM has not been verified experimentally. This mechanism [5–10], which gives mass to massive elementary particles, implies the existence of a scalar particle, the SM Higgs boson. The search for the Higgs boson is one of the highlights of the Large Hadron Collider [11] (LHC) physics programme.

Indirect limits on the SM Higgs boson mass of $m_H < 158 \text{ GeV}$ at 95% confidence level (CL) have been set using global fits to precision electroweak results [12]. Direct searches at LEP [13], the Tevatron [14–16] and the LHC [17, 18] have previously excluded, at 95% CL, a SM Higgs boson with mass below 600 GeV, apart from some mass regions between 116 GeV and 127 GeV.

Recently both the ATLAS and CMS Collaborations have reported the observation of a new particle in the search for the Higgs boson [19, 20]. The CDF and DØ experiments at the Tevatron have also recently reported a broad excess in the mass region 120–135 GeV with an observed local significance for $m_H = 125 \text{ GeV}$ of 2.8σ for the combination of the two experiments [16]. This talk covers the results reported in [19], as well as new results on the couplings of the newly observed particle reported in [21]. More complete discussion of these analyses is provided in these references.

The data taken are affected by multiple pp collisions occurring in the same or

neighbouring bunch crossings (pile-up). In the 7 TeV data, the average number of interactions per bunch crossing was ~ 10 , increasing to ~ 20 in the 8 TeV data. The reconstruction, identification and isolation criteria used for electrons and photons in the 8 TeV data are improved, making the $H \rightarrow ZZ^{(*)} \rightarrow 4\ell$ and $H \rightarrow \gamma\gamma$ searches more robust against the increased pile-up. These analyses were re-optimised with simulation and frozen before looking at the 8 TeV data.

In the $H \rightarrow WW^{(*)} \rightarrow \ell\nu\ell\nu$ channel, the increased pile-up deteriorates the event missing transverse momentum, E_T^{miss} , resolution, which results in significantly larger Drell-Yan background in the same-flavour final states. Since the $e\mu$ channel provides most of the sensitivity of the search, only this final state is used in the analysis of the 8 TeV data. The kinematic region in which a SM Higgs boson with a mass between 110 GeV and 140 GeV is searched for was kept blinded during the analysis optimisation, until satisfactory agreement was found between the observed and predicted numbers of events in control samples dominated by the principal backgrounds.

2 The ATLAS detector

The ATLAS detector [22] is a multi-purpose particle physics detector with approximately forward-backward symmetric cylindrical geometry. The inner tracking detector (ID) with a pseudo-rapidity coverage of $|\eta| < 2.5$ and consists of a silicon pixel detector, a silicon micro-strip detector, and a transition radiation tracker. The ID is surrounded by a thin superconducting solenoid providing a 2 T axial magnetic field. A high-granularity lead/liquid-argon (LAr) sampling calorimeter measures the energy and the position of electromagnetic showers within $|\eta| < 3.2$. LAr sampling calorimeters are also used to measure hadronic showers in the end-cap ($1.5 < |\eta| < 3.2$) and forward ($3.1 < |\eta| < 4.9$) regions, while an iron/scintillator tile calorimeter measures hadronic showers in the central region ($|\eta| < 1.7$). The muon spectrometer (MS) surrounds the calorimeters and consists of three large superconducting air-core toroid magnets, each with eight coils, a system of precision tracking chambers ($|\eta| < 2.7$), and fast tracking chambers for triggering. A three-level trigger system selects events to be recorded for offline analysis.

3 Signal and background simulation samples

The SM Higgs boson production processes considered in this analysis are the dominant gluon fusion ($gg \rightarrow H$, denoted ggF), vector-boson fusion ($qq' \rightarrow qq'H$, denoted VBF) and Higgs-strahlung ($qq' \rightarrow WH, ZH$, denoted WH/ZH). The small contribution from the associated production with a $t\bar{t}$ pair ($q\bar{q}/gg \rightarrow t\bar{t}H$, denoted $t\bar{t}H$) is taken into account only in the $H \rightarrow \gamma\gamma$ analysis. Full details on the simulation samples is provided in [19].

4 $H \rightarrow ZZ^{(*)} \rightarrow 4\ell$ channel

The search for the SM Higgs boson through the decay $H \rightarrow ZZ^{(*)} \rightarrow 4\ell$, where $\ell = e$ or μ , provides good sensitivity over a wide mass range (110-600 GeV) due

to a fully reconstructed final state with excellent momentum resolution allowing a peak to be seen above the background. This analysis searches for Higgs boson candidates by selecting two pairs of isolated leptons, each of which is comprised of two leptons with the same flavour and opposite charge. The expected cross section times branching ratio for the process $H \rightarrow ZZ^{(*)} \rightarrow 4\ell$ with Higgs mass hypothesis $m_H = 125$ GeV is 2.2 fb for $\sqrt{s} = 7$ TeV and 2.8 fb for $\sqrt{s} = 8$ TeV.

The largest background comes from continuum $(Z^{(*)}/\gamma^*)(Z^{(*)}/\gamma^*)$ production, referred to hereafter as $ZZ^{(*)}$. For low masses there are also important background contributions from Z +jets and $t\bar{t}$ production, where charged lepton candidates arise either from decays of hadrons with b - or c -quark content or from mis-identification of jets. The reducible backgrounds are suppressed with isolation and impact parameter requirements.

The crucial experimental aspects of this channel are:

- high lepton acceptance, reconstruction and identification down to low p_T ,
- good lepton energy/momentum resolution,
- good control of reducible backgrounds (Z +jets and $Z+b\bar{b}$ and $t\bar{t}$) in low mass region below ~ 170 GeV.

The reducible background estimates cannot rely on Monte Carlo (MC) simulation alone due to theoretical uncertainties and $b/\text{jet} \rightarrow \ell$ modeling. So the MC simulation is validated with data enriched control samples.

The 7 TeV data have been re-analysed and combined with the 8 TeV data. The analysis is improved in several aspects with respect to [23] to enhance the sensitivity to a low-mass Higgs boson. In particular, the kinematic selections are revised. The 8 TeV data analysis also benefits from improvements in the electron reconstruction and identification. The expected local signal significances for a Higgs boson with $m_H = 125$ GeV are 1.6σ for the 7 TeV data (to be compared with 1.25σ in [23]) and 2.1σ for the 8 TeV data.

4.1 Event selection

The data are selected using single-lepton or di-lepton triggers. Muon candidates are formed by matching reconstructed ID tracks with either a complete track or a track-segment reconstructed in the MS [24]. Electron candidates are formed from ID tracks pointing to electromagnetic calorimeter clusters, where the cluster must satisfy a set of identification criteria [25] that require the longitudinal and transverse shower profiles to be consistent with those expected for electromagnetic showers. The electron tracks are fitted using a Gaussian-Sum Filter [26], allowing for bremsstrahlung energy losses.

Quadruplets are formed from same-flavour opposite-charge (SFOC) lepton pairs with their transverse momentum, p_T , at least 20,15,10 GeV for the three leading leptons, and at least 7(6) GeV for the final muon (electron). The leading SFOC lepton pair has an invariant mass (m_{12}) closest to the Z boson mass with $50 \text{ GeV} < m_{12} < 106 \text{ GeV}$. The sub-leading SFOC lepton pair, with its invariant mass (m_{34}) required to be in the range $m_{\min} < m_{34} < 115 \text{ GeV}$ with m_{\min} varying

from 17.5 GeV at $m_{4\ell} = 120$ GeV to 50 GeV at $m_{4\ell} = 190$ GeV [27]. There are four different analysis sub-channels: $4e$, $2e2\mu$, $2\mu2e$ and 4μ , with the cross-flavoured pairs ordered in p_T .

Non-prompt leptons from heavy flavour decays, electrons from photon conversions and jets mis-identified as electrons have broader transverse impact parameter distributions than prompt leptons from Z boson decays and/or are non-isolated. Thus, the Z +jets and $t\bar{t}$ background contributions are reduced by applying a cut on the transverse impact parameter significance, d_0/σ_{d_0} , required to be less than 3.5 (6.5) for muons (electrons). In addition, leptons must satisfy isolation requirements based on tracking and calorimetric information. The normalised track isolation discriminant requires the sum of the transverse momenta of tracks inside a cone of size $\Delta R = 0.2$ around the lepton direction divided by the lepton p_T be smaller than 0.15. The normalised calorimetric isolation for electrons, the sum of the E_T of topological clusters [28] within $\Delta R = 0.2$ divided by the electron E_T , is required to be less than 0.2. Finally, the normalised calorimetric isolation discriminant for muons, the E_T sum of the calorimeter cells inside $\Delta R = 0.2$ divided by the muon p_T , is required to be less than 0.3.

The combined signal reconstruction and selection efficiencies for a SM Higgs with $m_H = 125$ GeV for the 7 TeV (8 TeV) data are 37% (36%) for the 4μ channel, 20% (22%) for the $2e2\mu/2\mu2e$ channels and 15% (20%) for the $4e$ channel.

The 4ℓ invariant mass resolution is improved by applying a Z -mass constrained kinematic fit to the leading lepton pair for $m_{4\ell} < 190$ GeV and to both lepton pairs for higher masses. The expected width of the reconstructed mass distribution is dominated by the experimental resolution for $m_H < 350$ GeV, and by the natural width of the Higgs boson for higher masses (30 GeV at $m_H = 400$ GeV). The typical mass resolutions for $m_H = 125$ GeV are 1.8 GeV, 2.0 GeV and 2.5 GeV for the 4μ , $2e2\mu/2\mu2e$ and $4e$ sub-channels, respectively.

4.2 Background estimation

The expected background yield and composition are estimated using the MC simulation normalised to the theoretical cross section for $ZZ^{(*)}$ production and by methods using control regions from data for the Z + jets and $t\bar{t}$ processes. Since the background composition depends on the flavour of the sub-leading lepton pair, different approaches are taken for the $\ell\ell + \mu\mu$ and the $\ell\ell + ee$ final states. The transfer factors needed to extrapolate the background yields from the control regions defined below to the signal region are obtained from the MC simulation. The MC description of the selection efficiencies for the different background components has been verified with data.

The reducible $\ell\ell + \mu\mu$ background is dominated by $t\bar{t}$ and Z +jets (mostly $Z+b\bar{b}$) events. A control region is defined by removing the isolation requirement on the leptons in the sub-leading pair, and by requiring that at least one of the sub-leading muons fails the transverse impact parameter significance selection. These modifications remove $ZZ^{(*)}$ contributions, and allow both the $t\bar{t}$ and Z + jets backgrounds to be estimated simultaneously using a fit to the m_{12} distribution (m_{12} peaks at m_Z for Z + jets and $t\bar{t}$ is relatively flat in m_{12}).

In order to estimate the reducible $\ell\ell + ee$ background, a control region is formed by relaxing the selection criteria for the electrons of the sub-leading pair. The different sources of electron background are then separated into categories consisting of non-prompt leptons from heavy flavour decays, electrons from photon conversions and jets mis-identified as electrons, using appropriate discriminating variables [29]. This method allows the sum of the $Z + \text{jets}$ and $t\bar{t}$ background contributions to be estimated. Two other methods have been used as cross-check and yield consistent results.

Table 1. Summary of the estimated numbers of $Z + \text{jets}$ and $t\bar{t}$ background events, for the 7 TeV and 8 TeV data in the entire phase-space of the analysis after the kinematic selections described in the text. The backgrounds are combined for the $2\mu 2e$ and $4e$ channels, as discussed in the text. The first uncertainty is statistical, while the second is systematic. Ref. [19].

Background	Estimated numbers of events	
	$\sqrt{s} = 7 \text{ TeV}$	$\sqrt{s} = 8 \text{ TeV}$
	4μ	
$Z + \text{jets}$	$0.3 \pm 0.1 \pm 0.1$	$0.5 \pm 0.1 \pm 0.2$
$t\bar{t}$	$0.02 \pm 0.02 \pm 0.01$	$0.04 \pm 0.02 \pm 0.02$
	$2e2\mu$	
$Z + \text{jets}$	$0.2 \pm 0.1 \pm 0.1$	$0.4 \pm 0.1 \pm 0.1$
$t\bar{t}$	$0.02 \pm 0.01 \pm 0.01$	$0.04 \pm 0.01 \pm 0.01$
	$2\mu 2e$	
$Z + \text{jets}, t\bar{t}$	$2.6 \pm 0.4 \pm 0.4$	$4.9 \pm 0.8 \pm 0.7$
	$4e$	
$Z + \text{jets}, t\bar{t}$	$3.1 \pm 0.6 \pm 0.5$	$3.9 \pm 0.7 \pm 0.8$

The data-driven background estimates are summarised in Table 1. The distribution of m_{34} , for events selected by the analysis except that the isolation and transverse impact parameter requirements for the sub-leading lepton pair are removed, is presented in Fig. 1.

4.3 Systematic uncertainties

The uncertainties on the integrated luminosities are determined to be 1.8% for the 7 TeV data and 3.6% for the 8 TeV data using the techniques described in [30].

The uncertainties on the lepton reconstruction and identification efficiencies and on the momentum scale and resolution are determined using samples of W , Z and J/ψ decays [24, 25]. The relative uncertainty on the signal acceptance due to the uncertainty on the muon reconstruction and identification efficiency is $\pm 0.7\%$ ($\pm 0.5\%/\pm 0.5\%$) for the 4μ ($2e2\mu/2\mu 2e$) channel for $m_{4\ell} = 600 \text{ GeV}$ and increases to $\pm 0.9\%$ ($\pm 0.8\%/\pm 0.5\%$) for $m_{4\ell} = 115 \text{ GeV}$. Similarly, the relative uncertainty on the signal acceptance due to the uncertainty on the electron reconstruction and identification efficiency is $\pm 2.6\%$ ($\pm 1.7\%/\pm 1.8\%$) for the $4e$ ($2e2\mu/2\mu 2e$) channel for $m_{4\ell} = 600 \text{ GeV}$ and reaches $\pm 8.0\%$ ($\pm 2.3\%/\pm 7.6\%$) for $m_{4\ell} = 115 \text{ GeV}$.

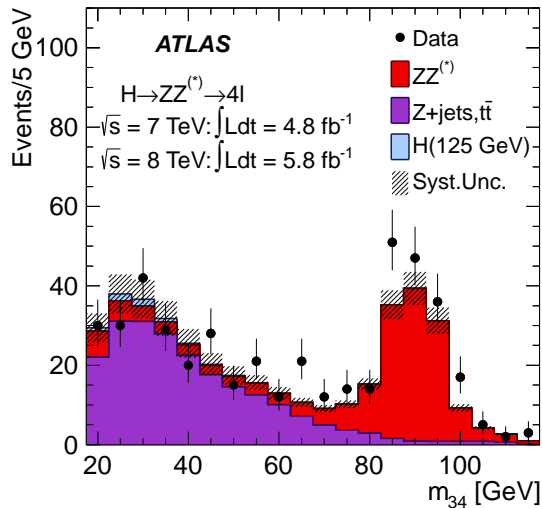


Figure 1. Invariant mass distribution of the sub-leading lepton pair (m_{34}) for a sample with of a Z boson candidate and an additional same-flavour electron or muon pair, for the combined 7 TeV and 8 TeV data after the kinematic selections described in the text. Isolation and transverse impact parameter significance requirements are applied to the leading lepton pair only. The MC is normalised to the data-driven background estimations. The relatively small contribution of a SM Higgs with $m_H = 125$ GeV in this sample is also shown. Ref. [19].

The uncertainty on the electron energy scale results in an uncertainty of $\pm 0.7\%$ ($\pm 0.5\%/\pm 0.2\%$) on the mass scale of the $m_{4\ell}$ distribution for the $4e$ ($2e2\mu/2\mu2e$) channel. The impact of the uncertainties on the electron energy resolution and on the muon momentum resolution and scale are found to be negligible.

The theoretical uncertainties associated with the signal are described in detail in [19].

4.4 Results

The expected distributions of $m_{4\ell}$ for the background and for a Higgs boson signal with $m_H = 125$ GeV are compared to the data in Fig. 2(a). The numbers of observed and expected events in a window of ± 5 GeV around $m_H = 125$ GeV are presented for the combined 7 TeV and 8 TeV data in Table 2. The distribution of the m_{34} versus m_{12} invariant mass is shown in Fig. 2(b). The statistical interpretation of the excess of events near $m_{4\ell} = 125$ GeV in Fig. 2(a) is presented in Section 9.

5 $H \rightarrow \gamma\gamma$ channel

The search for the SM Higgs boson through the decay $H \rightarrow \gamma\gamma$ is performed in the mass range between 110 GeV and 150 GeV. The dominant background is SM di-photon production ($\gamma\gamma$); contributions also come from γ +jet and jet+jet production

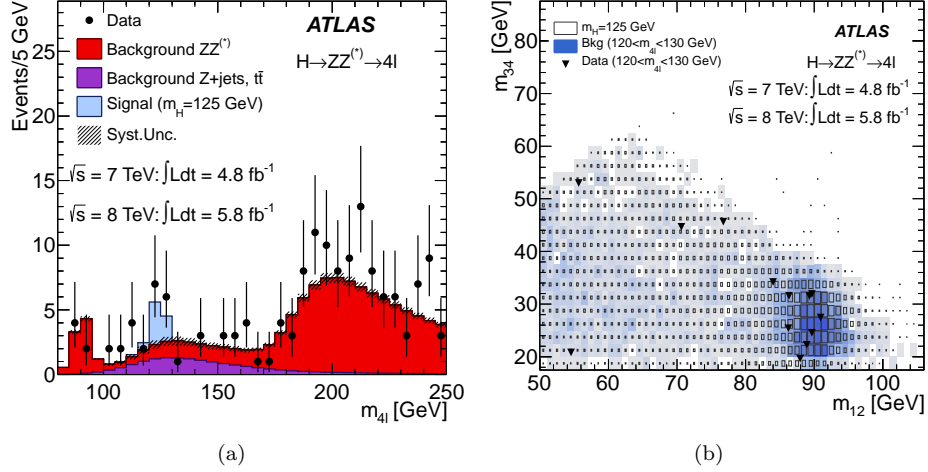


Figure 2. (a) The distribution of the four-lepton invariant mass, $m_{4\ell}$, for the selected candidates, compared to the background expectation in the 80–250 GeV mass range, for the combined 7 TeV and 8 TeV data. The signal expectation for a SM Higgs with $m_H = 125$ GeV is also shown. (b) The distribution of the m_{34} versus the m_{12} invariant mass, before the application of the Z -mass constrained kinematic fit, for the selected candidates in the $m_{4\ell}$ range 120–130 GeV. The expected distributions for a SM Higgs with $m_H = 125$ GeV (the sizes of the boxes indicate the relative density) and for the total background (the intensity of the shading indicates the relative density) are also shown. Ref. [19].

Table 2. The numbers of expected signal ($m_H = 125$ GeV) and background events, together with the numbers of observed events in the data, in a window of size ± 5 GeV around 125 GeV, for the combined 7 TeV and 8 TeV data. Ref. [19].

	Signal	$ZZ^{(*)}$	Z + jets, $t\bar{t}$	Observed
4μ	2.09 ± 0.30	1.12 ± 0.05	0.13 ± 0.04	6
$2e2\mu/2\mu2e$	2.29 ± 0.33	0.80 ± 0.05	1.27 ± 0.19	5
$4e$	0.90 ± 0.14	0.44 ± 0.04	1.09 ± 0.20	2

with one or two jets mis-identified as photons (γj and jj) and from the Drell-Yan process with the electrons mis-identified as photons. The 7 TeV data have been re-analysed and the results combined with those from the 8 TeV data. Among other changes to the analysis, a new category of events with two forward jets is introduced, which enhances the sensitivity to the VBF process. Overall, the sensitivity of the analysis has been improved by about 20% with respect to that described in [31].

5.1 Event selection

The data used in this channel are selected using a di-photon trigger [32], with $> 99\%$ efficiency after the final event selection. Events are required to contain

at least one reconstructed vertex with at least two tracks, as well as two photon candidates. Photon candidates must be in the fiducial region $|\eta| < 2.37$, excluding the calorimeter transition region $1.37 \leq |\eta| < 1.52$. Converted photons have one or two tracks matching the clusters in the calorimeter. The photon reconstruction efficiency is about 97% for $E_T > 30$ GeV.

MC simulation is used to calibrate for energy losses upstream of the calorimeter and leakage outside of the cluster of the photon candidates; this is done separately for unconverted and converted candidates. The calibration is refined by applying η -dependent correction factors ($\pm 1\%$) determined from measured $Z \rightarrow e^+e^-$ events. The leading (sub-leading) photon candidate is required to have $E_T > 40$ GeV (30 GeV).

Photon candidates must pass identification criteria based on shower shapes and hadronic energy leakage [33]. For the 7 TeV data, the selection uses a neural network, and for the 8 TeV data, cut-based criteria are used. This cut-based selection has been tuned to be robust against pile-up. The photon identification efficiencies range from 85% to above 95%. To further suppress the jet background, an isolation selection is applied by requiring the transverse energy of topological clusters within $\Delta R < 0.4$ to be less than 4 GeV.

5.2 Invariant mass reconstruction

The invariant mass of the two photons is evaluated using the photon energies measured in the calorimeter, the azimuthal angle ϕ between the photons as determined from the positions of the photons in the calorimeter, and the values of η calculated from the position of the identified primary vertex and the impact points of the photons in the calorimeter.

The primary vertex is identified by combining the following information in a global likelihood: the directions of flight of the photons as determined using the longitudinal segmentation of the electromagnetic calorimeter (calorimeter pointing), the parameters of the beam spot, and the $\sum p_T^2$ of the tracks associated with each reconstructed vertex. In addition, for the 7 TeV data analysis, the photon conversion vertex is used in the likelihood. The calorimeter pointing is sufficient to ensure that the contribution of the opening angle between the photons to the mass resolution is negligible. The tracking information from the ID improves the identification of the primary vertex, which is needed for the jet selection in the 2-jet category.

The number of selected di-photon candidates with an invariant mass between 100 GeV and 160 GeV is 23788 (35251) in the 7 TeV (8 TeV) data sample.

5.3 Event categorisation

To increase the sensitivity to a Higgs boson signal, the events are separated into ten mutually exclusive categories having different mass resolutions and signal-to-background ratios. An exclusive category of events containing two jets improves the sensitivity to VBF. The other nine categories are defined by the presence or

Table 3. Number of events in the data (N_D) and expected number of signal events (N_S) for $m_H = 126.5$ GeV from the $H \rightarrow \gamma\gamma$ analysis, for each category in the mass range 100–160 GeV. The mass resolution FWHM (see text) is also given for the 8 TeV data. The Higgs boson production cross section multiplied by the branching ratio into two photons ($\sigma \times B(H \rightarrow \gamma\gamma)$) is listed for $m_H = 126.5$ GeV. The statistical uncertainties on N_S and FWHM are less than 1%. Ref. [19].

\sqrt{s}	7 TeV		8 TeV		FWHM [GeV]
$\sigma \times B(H \rightarrow \gamma\gamma)$ [fb]	N_D	N_S	N_D	N_S	
Category	N_D	N_S	N_D	N_S	
Unconv. central, low p_{Tt}	2054	10.5	2945	14.2	3.4
Unconv. central, high p_{Tt}	97	1.5	173	2.5	3.2
Unconv. rest, low p_{Tt}	7129	21.6	12136	30.9	3.7
Unconv. rest, high p_{Tt}	444	2.8	785	5.2	3.6
Conv. central, low p_{Tt}	1493	6.7	2015	8.9	3.9
Conv. central, high p_{Tt}	77	1.0	113	1.6	3.5
Conv. rest, low p_{Tt}	8313	21.1	11099	26.9	4.5
Conv. rest, high p_{Tt}	501	2.7	706	4.5	3.9
Conv. transition	3591	9.5	5140	12.8	6.1
2-jet	89	2.2	139	3.0	3.7
All categories (inclusive)	23788	79.6	35251	110.5	3.9

not of converted photons, η of the selected photons, and p_{Tt} , the component^a of the di-photon p_T that is orthogonal to the axis defined by the difference between the two photon momenta [34, 35].

5.4 Signal modelling

The description of the Higgs boson signal is obtained from MC simulation. For both the 7 TeV and 8 TeV MC samples, the fractions of ggF, VBF, WH , ZH and $t\bar{t}H$ production are approximately 88%, 7%, 3%, 2% and 0.5%, respectively, for $m_H = 126.5$ GeV. The simulated shower shape distributions are shifted slightly to improve the agreement with the data [33], and the photon energy resolution is broadened (by approximately 1% (1.2–2.1%)) in the barrel (end-cap) calorimeter to account for small differences observed between $Z \rightarrow e^+e^-$ data and MC events. The signal yields expected for the 7 TeV and 8 TeV data samples are given in Table 3. The overall selection efficiency is about 40%.

The shape of the invariant mass of the signal in each category is modelled by the sum of a Crystal Ball function [36], describing the core of the distribution with a width σ_{CB} , and a Gaussian contribution describing the tails (amounting to <10%) of the mass distribution. The expected full-width-at-half-maximum (FWHM) is 3.9 GeV and σ_{CB} is 1.6 GeV for the inclusive sample, and varies with event category (see Table 3).

5.5 Background modelling

The background in each category is estimated from data by fitting the di-photon mass spectrum in the mass range 100–160 GeV with a selected model with free

^a $p_{Tt} = |(\mathbf{p}_1^{\gamma 1} + \mathbf{p}_1^{\gamma 2}) \times (\mathbf{p}_1^{\gamma 1} - \mathbf{p}_1^{\gamma 2})| / |\mathbf{p}_1^{\gamma 1} - \mathbf{p}_1^{\gamma 2}|$, where $\mathbf{p}_1^{\gamma 1}$ and $\mathbf{p}_1^{\gamma 2}$ are the transverse momenta of the two photons.

parameters of shape and normalisation. Different models are chosen for the different categories to achieve a good compromise between limiting the size of a potential bias while retaining good statistical power. The models are a fourth-order Bernstein polynomial function [37], an exponential function of a second-order polynomial and an exponential function. Based on MC studies, the background model which has the best sensitivity for $m_H = 125$ GeV and a bias less of than a 20% of the statistical uncertainty is chosen for each category. The largest absolute signal yield as defined above is taken as the systematic uncertainty on the background model, amounting to $\pm(0.2\text{--}4.6)$ and $\pm(0.3\text{--}6.8)$ events, depending on the category for the 7 TeV and 8 TeV data samples, respectively.

5.6 Systematic uncertainties

The dominant experimental uncertainty on the signal yield $\pm 8\%$ ($\pm 11\%$) for 7 TeV (8 TeV) data comes from the photon reconstruction and identification efficiency, which is estimated with data using electrons from Z decays and photons from $Z \rightarrow \ell^+ \ell^- \gamma$ events. The total uncertainty on the mass resolution is $\pm 14\%$. The dominant contribution ($\pm 12\%$) comes from the uncertainty on the energy resolution of the calorimeter, which is determined from $Z \rightarrow e^+ e^-$ events.

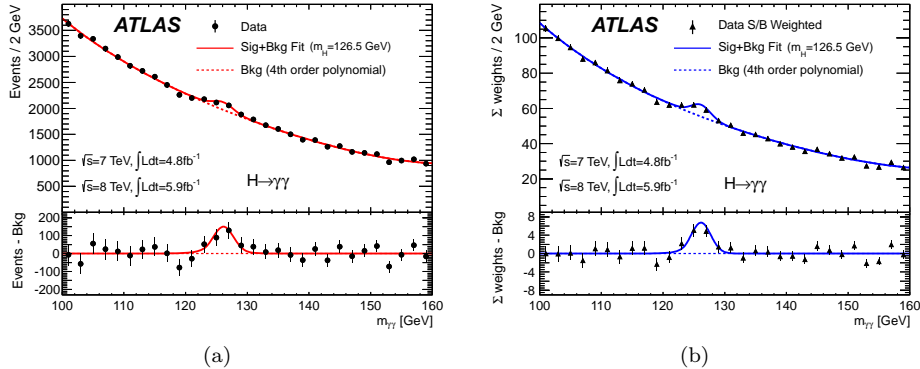


Figure 3. The distributions of the invariant mass of di-photon candidates after all selections for the combined 7 TeV and 8 TeV data sample. The inclusive sample is shown in (a) and a weighted version of the same sample in (b); the weights are explained in the text. The result of a fit to the data of the sum of a signal component fixed to $m_H = 126.5$ GeV and a background component described by a fourth-order Bernstein polynomial is superimposed. The residuals of the data and weighted data with respect to the respective fitted background component are also displayed. Ref. [19].

5.7 Results

The distribution of the invariant mass, $m_{\gamma\gamma}$, of the di-photon events, summed over all categories, is shown in Fig. 3(a). The result of a fit including a signal component

fixed to $m_H = 126.5$ GeV and a background component described by a fourth-order Bernstein polynomial is superimposed.

The statistical analysis uses an unbinned likelihood function constructed from those of the ten categories of the 7 TeV and 8 TeV data samples. To demonstrate the sensitivity of this likelihood analysis, Fig. 3(b) also shows the mass spectrum obtained after weighting events with category-dependent factors reflecting the signal-to-background ratios. The statistical interpretation of the excess of events near $m_{\gamma\gamma} = 126.5$ GeV in Fig. 3 is presented in Section 9.

6 $H \rightarrow WW^{(*)} \rightarrow e\nu\mu\nu$ channel

The signature for the $H \rightarrow WW^{(*)} \rightarrow \ell\nu\ell\nu$ channel is two opposite-charge leptons with large transverse momentum and a large momentum imbalance in the event due to the escaping neutrinos. This channel has a high rate, but limited mass resolution. The dominant backgrounds are non-resonant WW and top production, both of which have real W pairs in the final state. Other important backgrounds include Drell-Yan events ($Z/\gamma^{(*)} \rightarrow \ell\ell$) with mis-measured E_T^{miss} , W +jets events with a fake second lepton, and $W\gamma$ events with an electron from a conversion.

The analysis of the 8 TeV data is restricted to the $e\mu$ final state, providing $> 85\%$ of the sensitivity of the search, due to the higher luminosity and increased number of interactions which worsens the Drell-Yan background. The Drell-Yan background to the $e\mu$ final state is from semi-lepton τ decays and thus significantly reduced.

6.1 Event selection

For the 8 TeV $H \rightarrow WW^{(*)} \rightarrow e\nu\mu\nu$ search, the data are selected using inclusive single-muon and single-electron triggers. Candidates are selected with a leading (sub-leading) lepton $E_T > 25$ GeV (> 15 GeV). The lepton selection and isolation have more stringent requirements than those used for the $H \rightarrow ZZ^{(*)} \rightarrow 4\ell$ analysis (see Section 4), to reduce the larger background from non-prompt leptons in the $\ell\nu\ell\nu$ final state. Events are separated into 0, 1 and 2-jet categories, with $p_T^{\text{jet}} > 25(30)$ GeV for $|\eta| < 2.5$ ($2.5 - 4.5$).

With two neutrinos in the signal final state, events are required to have large E_T^{miss} . The quantity $E_{T,\text{rel}}^{\text{miss}}$ is required to be > 25 GeV and is the projection of the direction of E_T^{miss} perpendicular to the nearest lepton or jet. Compared to E_T^{miss} , $E_{T,\text{rel}}^{\text{miss}}$ has increased rejection power when the E_T^{miss} is generated by a neutrino in a jet or the mis-measurement of an object.

The data are subdivided into 0-jet, 1-jet and 2-jet search channels since the background rate and composition depend significantly on the jet multiplicity. The 0-jet background is dominated by WW events, and top is an important background for the other two channels. To reduce the WW background, the di-leptons are required to be close together ($|\Delta\phi_{\ell\ell}| < 1.8$), which arises from the spin-0 of a SM Higgs and the V-A nature of the W decay. Top backgrounds are reduced with b -tagging requirements. Further details on the event selection can be found in [19]. For $m_H = 125$ GeV, the combined acceptance times efficiency of the 8 TeV 0-jet and

1-jet selection is about 7.4%.

6.2 Background normalisation and control samples

The leading backgrounds from SM processes producing two isolated high- p_T leptons and E_T^{miss} are WW and top, both $t\bar{t}$ and single top. These are estimated using partially data-driven techniques based on normalising the MC predictions to the data in control regions dominated by the relevant background source. The W +jets background is estimated from data for all jet multiplicities. Only the small backgrounds from Drell-Yan and di-boson processes other than WW , as well as the WW background for the 2-jet analysis, are estimated using MC simulation.

The control regions are defined by selections similar to those used for the signal region but with some criteria reversed or modified to obtain signal-depleted samples enriched in a particular background. Some control regions have significant contributions from backgrounds other than the targeted one, which introduces dependencies among the background estimates. These correlations are taken into account in the WW control region where the top and W +jets backgrounds are subtracted using their respective measurements. See [19] for full details on the background control samples and estimates.

6.3 Systematic uncertainties

The systematic uncertainties that have the largest impact on the sensitivity of the search are the theoretical uncertainties associated with the signal, arising from the separation into 0-,1-,and 2-jet channels. The main experimental uncertainties are associated with the JES, the jet energy resolution (JER), pile-up, E_T^{miss} , the b -tagging efficiency, the W +jets transfer factor, and the integrated luminosity. The largest uncertainties on the backgrounds include WW normalisation and modelling, top normalisation, and $W\gamma^{(*)}$ normalisation. The 2-jet systematic uncertainties are dominated by the statistical uncertainties in the data and the MC simulation.

Table 4. The expected numbers of signal ($m_H = 125$ GeV) and background events after all selections, including a cut on the transverse mass of $0.75 m_H < m_T < m_H$ for $m_H = 125$ GeV. The observed numbers of events in data are also displayed. The uncertainties shown are the combination of the statistical and all systematic uncertainties, taking into account the constraints from control samples. For the 2-jet analysis, backgrounds with fewer than 0.01 expected events are marked with ‘-’. Ref. [19].

	0-jet	1-jet	2-jet
Signal	20 ± 4	5 ± 2	0.34 ± 0.07
WW	101 ± 13	12 ± 5	0.10 ± 0.14
$WZ^{(*)}/ZZ/W\gamma^{(*)}$	12 ± 3	1.9 ± 1.1	0.10 ± 0.10
$t\bar{t}$	8 ± 2	6 ± 2	0.15 ± 0.10
$tW/tb/tqb$	3.4 ± 1.5	3.7 ± 1.6	-
$Z/\gamma^* + \text{jets}$	1.9 ± 1.3	0.10 ± 0.10	-
$W + \text{jets}$	15 ± 7	2 ± 1	-
Total Background	142 ± 16	26 ± 6	0.35 ± 0.18
Observed	185	38	0

6.4 Results

Table 4 shows the numbers of events expected from a SM Higgs boson with $m_H = 125$ GeV and from the backgrounds, as well as the numbers of candidates observed in data, after application of all selection criteria plus an additional cut on m_T of $0.75 m_H < m_T < m_H$. The uncertainties shown in Table 4 combine statistical and systematic uncertainties. An excess of events relative to the background expectation is observed in the data.

Figure 4 shows the distribution of the transverse mass after all selection criteria in the 0-jet and 1-jet channels combined. The statistical interpretation of the observed excess of events is presented in Section 9.

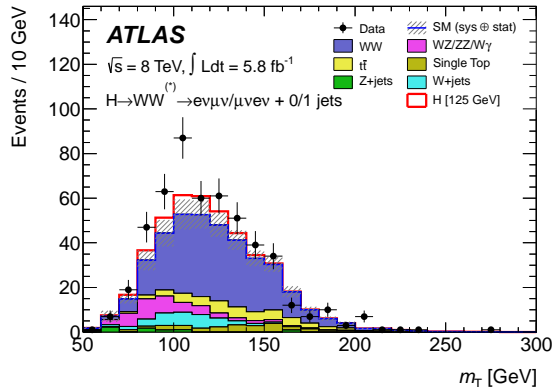


Figure 4. Distribution of the transverse mass, m_T , in the 0-jet and 1-jet analyses, for events satisfying all selection criteria. The expected signal for $m_H = 125$ GeV is shown stacked on top of the background prediction. The W +jets background is estimated from data, and WW and top background MC predictions are normalised to the data using control regions. The hashed area indicates the total uncertainty on the background prediction. Ref. [19].

7 Statistical procedure

The parameter of interest is the global signal strength factor μ , which is a scale factor on the total number of events predicted for a SM Higgs boson signal, defined such that $\mu = 0$ corresponds to the background-only hypothesis and $\mu = 1$ corresponds to the SM Higgs boson signal plus background. Hypothesised values of μ are tested with a statistic $\lambda(\mu)$ based on the profile likelihood ratio [38]. This test statistic extracts the information on the signal strength from a full likelihood fit to the data, including all systematic uncertainties and their correlations.

Exclusion limits are based on the CL_s prescription [39]; a value of μ is excluded at 95% CL when CL_s is less than 5%. A SM Higgs boson mass m_H is excluded at 95% CL when $\mu = 1$ is excluded at that mass. The significance of an excess in the data is first quantified with the local p_0 , the probability that the background can produce a fluctuation greater than the excess observed in data. The equivalent formulation in terms of number of standard deviations, Z_l , is referred to as the local

significance. The global probability for the most significant excess to be observed anywhere in a given search region includes a correction for the “look elsewhere” effect, reducing that given by local p_0 .

8 Correlated systematic uncertainties

The full list of the individual search channels that enter the combination are provided in [19]. The main uncorrelated systematic uncertainties correspond to the elements of the background estimates. The sources of correlated systematic uncertainties are: integrated luminosity, electron/photon energy scales, muon reconstruction, JES and E_T^{miss} , and theoretical uncertainties.

9 Results

The addition of the 8 TeV data for the $H \rightarrow ZZ^{(*)} \rightarrow 4\ell$, $H \rightarrow \gamma\gamma$ and $H \rightarrow WW^{(*)} \rightarrow e\nu\mu\nu$ channels, as well as the improvements to the analyses of the 7 TeV data in the first two of these channels, bring a significant gain in sensitivity in the low-mass region with respect to the previous combined search [17].

9.1 Excluded mass regions

The combined 95% CL exclusion limits on the production of the SM Higgs boson, expressed in terms of the signal strength parameter μ , are shown in Fig. 5(a) as a function of m_H . The expected 95% CL exclusion region covers the m_H range from 110 GeV to 582 GeV. The observed 95% CL exclusion regions are 111–122 GeV and 131–559 GeV. Three mass regions are excluded at 99% CL, 113–114, 117–121 and 132–527 GeV, while the expected exclusion range at 99% CL is 113–532 GeV.

Table 5. Characterisation of the excess in the $H \rightarrow ZZ^{(*)} \rightarrow 4\ell$, $H \rightarrow \gamma\gamma$ and $H \rightarrow WW^{(*)} \rightarrow \ell\nu\ell\nu$ channels and the combination of all channels. The mass value m_{max} for which the local significance is maximum, the maximum observed local significance Z_l and the expected local significance $E(Z_l)$ in the presence of a SM Higgs boson signal at m_{max} are given. The best fit value of the signal strength parameter $\hat{\mu}$ at $m_H = 126$ GeV is shown with the total uncertainty. The expected and observed mass ranges excluded at 95% CL (99% CL, indicated by a *) are also given, for the combined 7 TeV and 8 TeV data. Ref. [19].

Search channel	Dataset	m_{max} [GeV]	Z_l [σ]	$E(Z_l)$ [σ]	$\hat{\mu}(m_H = 126 \text{ GeV})$	Expected exclusion [GeV]	Observed exclusion [GeV]
$H \rightarrow ZZ^{(*)} \rightarrow 4\ell$	7 TeV	125.0	2.5	1.6	1.4 ± 1.1		
	8 TeV	125.5	2.6	2.1	1.1 ± 0.8		
	7 & 8 TeV	125.0	3.6	2.7	1.2 ± 0.6	124–164, 176–500	131–162, 170–460
$H \rightarrow \gamma\gamma$	7 TeV	126.0	3.4	1.6	2.2 ± 0.7		
	8 TeV	127.0	3.2	1.9	1.5 ± 0.6		
	7 & 8 TeV	126.5	4.5	2.5	1.8 ± 0.5	110–140	112–123, 132–143
$H \rightarrow WW^{(*)} \rightarrow \ell\nu\ell\nu$	7 TeV	135.0	1.1	3.4	0.5 ± 0.6		
	8 TeV	120.0	3.3	1.0	1.9 ± 0.7		
	7 & 8 TeV	125.0	2.8	2.3	1.3 ± 0.5	124–233	137–261
Combined	7 TeV	126.5	3.6	3.2	1.2 ± 0.4		
	8 TeV	126.5	4.9	3.8	1.5 ± 0.4		
	7 & 8 TeV	126.5	6.0	4.9	1.4 ± 0.3	110–582 113–532 (*)	111–122, 131–559 113–114, 117–121, 132–527 (*)

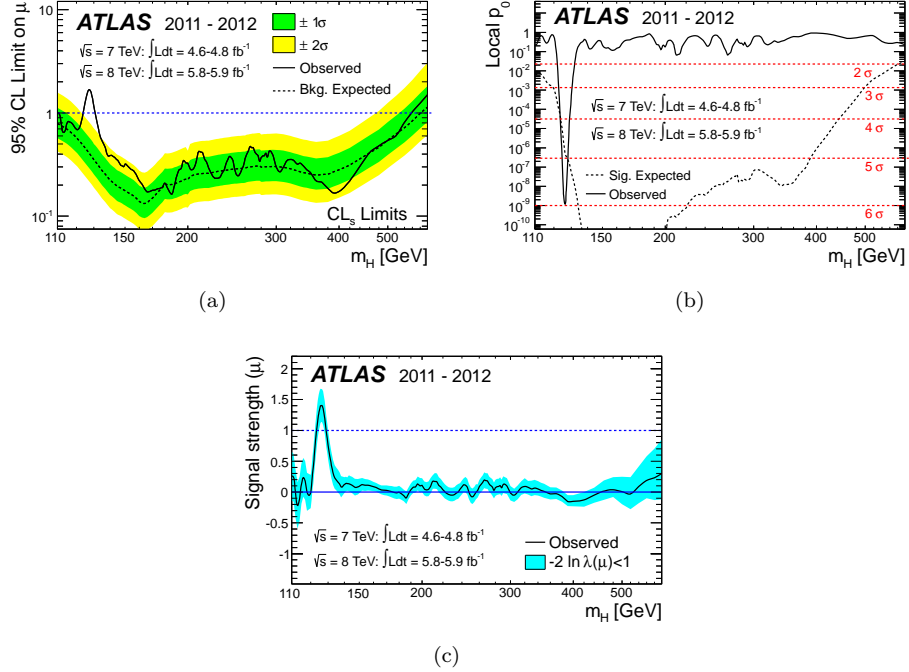


Figure 5. Combined search results: (a) The observed (solid) 95% CL limits on the signal strength as a function of m_H and the expectation (dashed) under the background-only hypothesis. The dark and light shaded bands show the $\pm 1\sigma$ and $\pm 2\sigma$ uncertainties on the background-only expectation. (b) The observed (solid) local p_0 as a function of m_H and the expectation (dashed) for a SM Higgs boson signal hypothesis ($\mu = 1$) at the given mass. (c) The best-fit signal strength $\hat{\mu}$ as a function of m_H . The band indicates the approximate 68% CL interval around the fitted value. Ref. [19].

9.2 Observation of an excess of events

An excess of events is observed near $m_H = 126$ GeV in the $H \rightarrow ZZ^{(*)} \rightarrow 4\ell$ and $H \rightarrow \gamma\gamma$ channels, both of which provide fully reconstructed candidates with high resolution in invariant mass, as shown in Figures 6(a) and 6(b). These excesses are confirmed by the highly sensitive but low-resolution $H \rightarrow WW^{(*)} \rightarrow \ell\nu\ell\nu$ channel, as shown in Fig. 6(c).

The observed local p_0 values from the combination of channels, using the asymptotic approximation, are shown as a function of m_H in Fig. 5(b) for the full mass range and in Fig. 7(a) for the low mass range, shown as a function of time.

The largest local significance for the combination of the 7 and 8 TeV data is found for a SM Higgs boson mass hypothesis of $m_H = 126.5$ GeV, where it reaches 6.0σ , with an expected value at that mass of 4.9σ (see also Table 5). For the 2012 data alone, the maximum local significance for the $H \rightarrow ZZ^{(*)} \rightarrow 4\ell$, $H \rightarrow \gamma\gamma$ and $H \rightarrow WW^{(*)} \rightarrow \ell\nu\ell\nu$ channels combined is 4.9σ , and occurs at $m_H = 126.5$ GeV (3.8σ expected). Including electron/photon energy resolution and scale systematic uncertainties, as described in [40], reduces the local significance to 5.9σ . The global significance of a local 5.9σ excess anywhere in the mass range 110–600 GeV

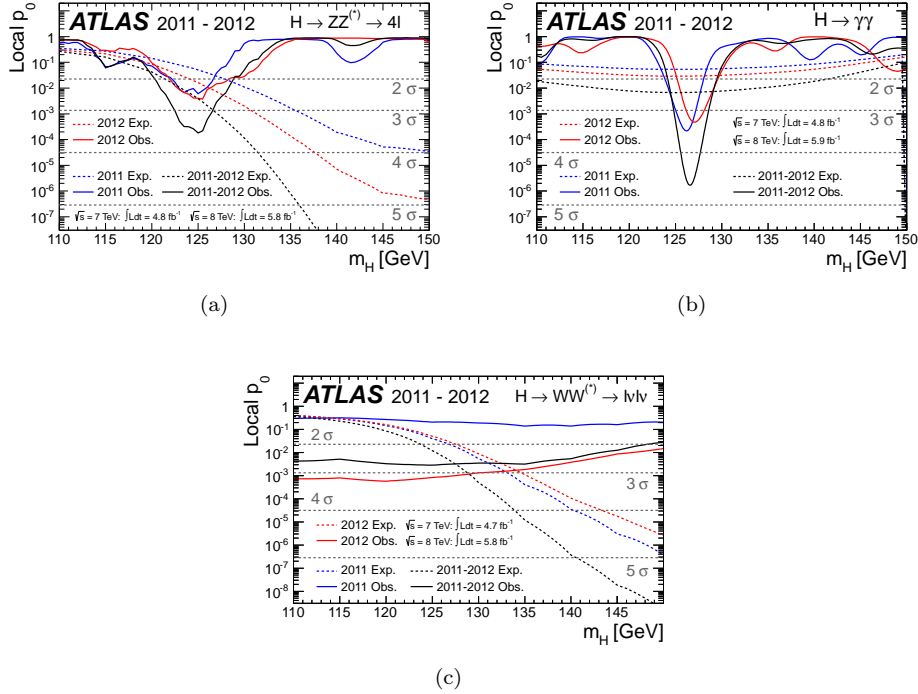


Figure 6. The observed local p_0 as a function of the hypothesised Higgs boson mass for the (a) $H \rightarrow ZZ^{(*)} \rightarrow 4\ell$, (b) $H \rightarrow \gamma\gamma$ and (c) $H \rightarrow WW^{(*)} \rightarrow \ell\nu\ell\nu$ channels. The dashed curves show the expected local p_0 under the hypothesis of a SM Higgs boson signal at that mass. Results are shown separately for the 7 TeV data (dark blue), the 8 TeV data (light red), and their combination (black). Ref. [19].

is estimated to be approximately 5.1σ .

9.3 Characterising the excess

The mass of the observed new particle is estimated using the profile likelihood ratio $\lambda(m_H)$ for $H \rightarrow ZZ^{(*)} \rightarrow 4\ell$ and $H \rightarrow \gamma\gamma$, the two channels with the highest mass resolution. The signal strength is allowed to vary independently in the two channels, although the result is essentially unchanged when restricted to the SM hypothesis $\mu = 1$. The leading sources of systematic uncertainty come from the electron and photon energy scales and resolutions. The resulting estimate for the mass of the observed particle is 126.0 ± 0.4 (stat) ± 0.4 (sys) GeV.

The best-fit signal strength $\hat{\mu}$ is shown in Fig. 5(c) as a function of m_H . The observed excess corresponds to $\hat{\mu} = 1.4 \pm 0.3$ for $m_H = 126$ GeV, consistent with the SM Higgs boson hypothesis $\mu = 1$. A summary of the individual and combined best-fit values of the strength parameter for a SM Higgs boson mass hypothesis of 126 GeV is shown in Fig. 7(b), while more information about the three main channels is provided in Table 5.

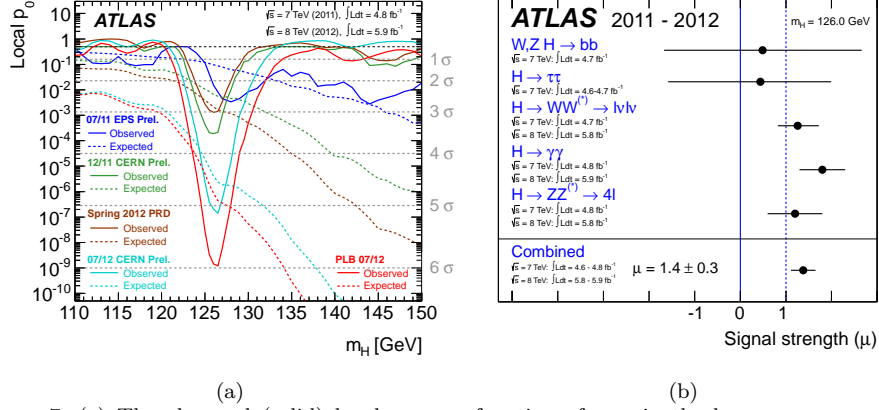


Figure 7. (a) The observed (solid) local p_0 as a function of m_H in the low mass range. The dashed curve shows the expected local p_0 under the hypothesis of a SM Higgs boson signal at that mass with its $\pm 1\sigma$ band. Results are shown as a function of time. The different sets of lines The horizontal dashed lines indicate the p -values corresponding to significances of 1 to 6σ . (b) Measurements of the signal strength parameter μ for $m_H = 126$ GeV for the individual channels and their combination. Ref. [19].

The observed production and decays modes allow the SM Higgs couplings to be probed [21] with a few simple assumptions: a single resonance with $m_H = 126$ GeV, SM Higgs $J^{CP} (0^{++})$, and a negligible width (i.e. $\sigma \times BR(ii \rightarrow H \rightarrow ff) = \sigma_{ii} \times \Gamma_{ff} / \Gamma_H$ for initial/final states i/f). Compatibility of with a SM Higgs interpretation can be expressed by scale factors κ_i such that $\sigma_{ii} / \sigma_{SM} = \Gamma_{ii} / \Gamma_{SM} = \kappa_i^2$. Figure 8 shows the κ_i likelihood fit results for three simplifying assumptions. Fig. 8(a) shows κ_F vs κ_V assuming a single scale factor for all fermions and for all vector couplings. The 68% CL intervals when profiling over all other parameters are: $\kappa_F \in [-1.0, 0.7] \cup [0.7, 1.3]$, $\kappa_V \in [0.9, 1.0] \cup [1.1, 1.3]$. Fig. 8(b) shows the ratio of W to Z couplings $\lambda_{WZ} = \kappa_W / \kappa_Z$. These scale factors are required to be identical within tight bounds by $SU(2)_V$ custodial symmetry and the ρ parameter measurements at LEP [12]. The fitted ratio is: $\lambda_{WZ} = 1.07^{+0.35}_{-0.27}$. Finally, Fig. 8(c) shows an invisible or undetectable branching ratio when allowing κ_g and κ_γ to vary, providing at 68% CL $BR_{inv.,undet.} < 0.68$. No significant deviation from SM expectations is found.

10 Conclusion

Searches for the SM Higgs boson have been performed in the $H \rightarrow ZZ^{(*)} \rightarrow 4\ell$, $H \rightarrow \gamma\gamma$ and $H \rightarrow WW^{(*)} \rightarrow e\nu\mu\nu$ channels with the ATLAS experiment at the LHC using 5.8–5.9 fb^{-1} of pp collision data recorded in 2012 at 8 TeV. These results are combined with earlier results [17], which are based on an integrated luminosity of 4.6–4.8 fb^{-1} recorded in 2011 at 7 TeV, except for the $H \rightarrow ZZ^{(*)} \rightarrow 4\ell$ and $H \rightarrow \gamma\gamma$ channels, which have been updated with the improved analyses.

The SM Higgs boson is excluded at 95% CL in the mass range 111–559 GeV,

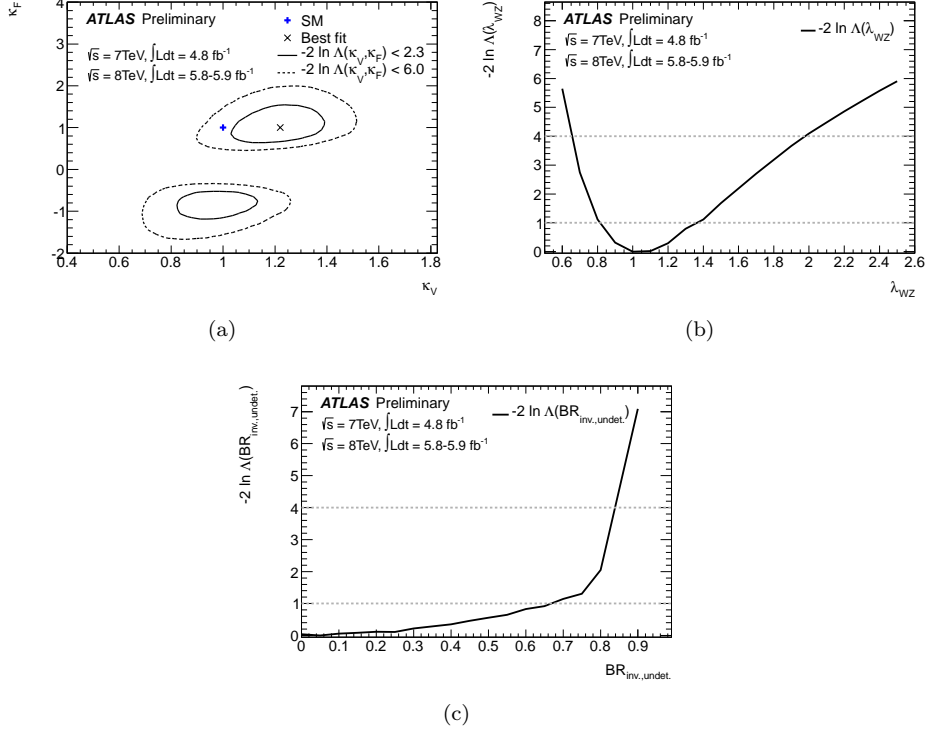


Figure 8. (a) Fit for different coupling strengths for fermions and vector bosons, assuming no non-SM contribution to the total width; (b) fit probing deviations in the vector sector; (c) fit of invisible or undetectable branching ratio when probing $gg \rightarrow H$ and $H \rightarrow \gamma\gamma$ loops. The contours and horizontal dashed lines correspond to the 68% and 95% CL. Ref. [21].

except for the narrow region 122–131 GeV. In this region, an excess of events with a local significance 5.9σ , corresponding to $p_0 = 1.7 \times 10^{-9}$, is observed. The excess is driven by the two channels with the highest mass resolution, $H \rightarrow ZZ^{(*)} \rightarrow 4\ell$ and $H \rightarrow \gamma\gamma$, and the equally sensitive but low-resolution $H \rightarrow WW^{(*)} \rightarrow \ell\nu\ell\nu$ channel. Taking into account the entire mass range of the search, 110–600 GeV, the global significance of the excess is 5.1σ , which corresponds to $p_0 = 1.7 \times 10^{-7}$.

These results provide conclusive evidence for the discovery of a new particle with mass $126.0 \pm 0.4(\text{stat}) \pm 0.4(\text{sys})$ GeV. The signal strength parameter μ has the value 1.4 ± 0.3 at the fitted mass, which is consistent with the SM Higgs boson hypothesis $\mu = 1$. The decays to pairs of vector bosons whose net electric charge is zero identify the new particle as a neutral boson. The observation in the di-photon channel disfavors the spin-1 hypothesis [41,42]. Tests of the production and decay couplings with simplifying assumptions find that these results are compatible with the hypothesis that the new particle is the SM Higgs boson, and more data are needed to assess its nature in detail.

References

1. S. L. Glashow, Nucl. Phys. **22** no. 4, (1961) 579.
2. S. Weinberg, Phys. Rev. Lett. **19** (1967) 1264.
3. A. Salam, *Elementary particle theory: relativistic groups and analyticity*, N. Svartholm, ed., p. 367. Almqvist & Wiksell, 1968. Proceedings of the eighth Nobel symposium.
4. G. 't Hooft and M. Veltman, Nucl. Phys. **B44** (1972) 189.
5. F. Englert and R. Brout, Phys. Rev. Lett. **13** (1964) 321.
6. P. W. Higgs, Phys. Lett. **12** (1964) 132.
7. P. W. Higgs, Phys. Rev. Lett. **13** (1964) 508.
8. G. S. Guralnik, C. R. Hagen, and T. W. B. Kibble, Phys. Rev. Lett. **13** (1964) 585.
9. P. W. Higgs, Phys. Rev. **145** (1966) 1156.
10. T. W. B. Kibble, Phys. Rev. **155** (1967) 1554.
11. L. Evans and P. Bryant (Eds.), JINST **3** (2008) S08001.
12. ALEPH, CDF, DØ, DELPHI, L3, OPAL, SLD Collaborations, the LEP Electroweak Working Group, the Tevatron Electroweak Working Group, and the SLD electroweak and heavy flavour groups, CERN-PH-EP-2010-095 (2010), [arXiv:1012.2367](https://arxiv.org/abs/1012.2367) [[hep-ex](#)].
13. ALEPH, DELPHI, L3 and OPAL Collaborations, The LEP Working Group for Higgs boson searches, Phys. Lett. **B 565** (2003) 61.
14. CDF Collaboration, T. Aaltonen et al., Phys. Rev. Lett. **109** (2012) 111802, [arXiv:1207.1707](https://arxiv.org/abs/1207.1707) [[hep-ex](#)].
15. DØ Collaboration, V. M. Abazov et al., Phys. Rev. Lett. **109** (2012) 121802, [arXiv:1207.6631](https://arxiv.org/abs/1207.6631) [[hep-ex](#)].
16. CDF Collaboration, DØ Collaboration, Phys. Rev. Lett. **109** (2012) 71804, Lett. (2012), [arXiv:1207.6436](https://arxiv.org/abs/1207.6436) [[hep-ex](#)].
17. ATLAS Collaboration, Phys. Rev. **D86** (2012) 032003.
18. CMS Collaboration, Phys. Lett. **B 710** (2012) 26.
19. ATLAS Collaboration, Phys. Lett. **B716** (2012) 1–29, [arXiv:1207.7214](https://arxiv.org/abs/1207.7214) [[hep-ex](#)]. Figures from ATLAS web.
20. CMS Collaboration, Phys. Lett. **B716** (2012) 30–61, [arXiv:1207.7235](https://arxiv.org/abs/1207.7235) [[hep-ex](#)].
21. ATLAS Collaboration, ATLAS-CONF-2012-127 (2012) <http://cdsweb.cern.ch/record/1476765>.
22. ATLAS Collaboration, JINST **3** (2008) S08003.
23. ATLAS Collaboration, Phys. Lett. **B 710** (2012) 383.
24. ATLAS Collaboration, ATLAS-CONF-2011-063 (2011) <http://cdsweb.cern.ch/record/1345743>.
25. ATLAS Collaboration, Eur. Phys. J. **C72** (2012) 1909.
26. ATLAS Collaboration, ATLAS-CONF-2012-047 (2012) <http://cdsweb.cern.ch/record/1449796>.
27. ATLAS Collaboration, ATLAS-CONF-2012-092 (2012) <http://cdsweb.cern.ch/record/1460411>.
28. W. Lampl, S. Laplace, D. Lelas, P. Loch, H. Ma, S. Menke, S. Rajagopalan,

- D. Rousseau, S. Snyder, and G. Unal, ATL-LARG-PUB-2008-002 (2008)
<http://cdsweb.cern.ch/record/1099735>.
29. ATLAS Collaboration, Phys. Lett. **B 707** (2012) 438.
 30. ATLAS Collaboration, ATLAS-CONF-2012-080 (2012)
<http://cdsweb.cern.ch/record/1460392>.
 31. ATLAS Collaboration, Phys. Rev. Lett. **108** (2012) 111803.
 32. ATLAS Collaboration, Eur. Phys. J. **C72** (2012) 1849.
 33. ATLAS Collaboration, Phys. Rev. **D83** (2011) 052005.
 34. OPAL Collaboration Collaboration, K. Ackerstaff et al., Eur. Phys. J. **C4** (1998) 47, [arXiv:hep-ex/9710010](https://arxiv.org/abs/hep-ex/9710010) [hep-ex].
 35. M. Vesterinen and T. R. Wyatt, Nucl. Instrum. Meth. **A602** (2009) 432.
 36. J. Gaiser, Ph.D. Thesis No. SLAC-R-255, (1982) 178.
 37. S. N. Bernstein, Comm. Soc. Math. Kharkov **13** (1912) 1.
 38. G. Cowan, K. Cranmer, E. Gross, and O. Vitells, Eur. Phys. J. **C71** (2011) 1554.
 39. A. L. Read, J. Phys. **G28** (2002) 2693.
 40. ATLAS Collaboration, ATLAS-CONF-2012-093 (2012)
<http://cdsweb.cern.ch/record/1460439>.
 41. L. D. Landau, Dokl. Akad. Nauk. **USSR 60** (1948) 207.
 42. C. N. Yang, Phys. Rev. **77** (1950) 242.